Acoustic Phenomena in Damaged Ceramic Capacitors

Saku Levikari, Tommi J. Kärkkäinen, *Member, IEEE*, Caroline Andersson, *Member, IEEE*, Juha Tamminen, and Pertti Silventoinen, *Member, IEEE*

***Abstract*—Multilayer ceramic capacitors are prone to mechanical defects and damage because of the fragility of the ceramic dielectric. Because these faults are often not recognized by visual or electrical inspection, a nondestructive fast way of detecting these defects would be very useful. Ceramic capacitors are known to generate acoustic emissions, caused by mechanical vibration of the capacitor body. Physical defects alter the mechanical properties of the capacitor, which, in turn, affect the acoustic signature of the capacitor. In this paper, acoustic information is acquired directly from both pristine and damaged capacitors. An experiment was conducted where capacitors were driven with a voltage chirp over a wide range of frequencies, and subsequent acoustic emissions were measured with a piezoelectric point contact sensor. Test boards were bent to cause flex cracks to the soldered capacitors, which were measured acoustically before and after bending. A comparison of these measurements showed that printed circuit board bending causes characteristic changes to the capacitor acoustic response, which can be correlated with the resulted damage.**

***Index Terms*—Acoustic emission, ceramic capacitors, nondestructive testing.**

I. Introduction

MULTILAYER ceramic capacitors (MLCCs) are widely used in the electronics industry because of their high capacitance per volume and favorable electrical characteristics [1]. The ceramic dielectric yields high permittivity, but also makes the MLCCs prone to cracks.

Typical defects in MLCCs are voids and delaminations, often related to thermal stresses during manufacturing [2], [3]. Flex cracks [4] (see Fig. 1) are another typical defect, often resulting from mechanical force exerted on the capacitor during circuit board handling or assembly [5], [6]. A cracked capacitor is often not recognized during the production or assembly, as it may operate normally, and defects cannot be detected by visual inspection. In the field, however, the crack may shorten the lifespan of the capacitor, reduce the capacitance, or cause a total failure of the component (an open or short contact) [7]. Hence, there is a need for detecting these defects before the product is delivered to the customer. Mechanical microsectioning [8] and chemical etching [9] are destructive methods for accurate defect detection in MLCCs, the former being the more usual method. Acoustic microscopy [6] is a commonly used nondestructive method; other studied techniques include acoustic emission stimulation using a mechanical ram [7], impedance analysis under dc bias (measurement of electromechanical resonances) [10], phase analysis using tone-burst excitation [11], leakage current monitoring [12], laser speckle pattern analysis [13], optoacoustic microscopy [14], and neutron radiography [15]. Recently, an X-ray imaging method with sufficient accuracy for reliable detection of flex cracks was demonstrated [16]. Krieger *et al.* used an audio range microphone to detect acoustic emissions caused by an MLCC on a printed circuit board (PCB) and observed differences between the signatures of intact and cracked capacitors [12]. Ko *et al.* showed that the fundamental resonant frequencies of a typical MLCC are in the order of 1 MHz [1] and, hence, cannot be observed directly using an audio-range microphone. Erdahl and Ume used laser interferometry to detect changes in the vibrations of an MLCC, observing an amplitude increase in damaged capacitors [17], [18].

Later on, amplitude increases [19] and frequency shifts [20] in MLCC acoustic resonances have been observed using reso-

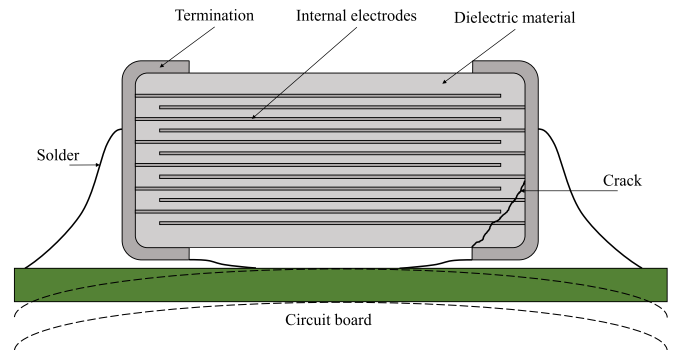

Fig. 1. Structure of a typical MLCC with a crack in the dielectric material cutting a part of the inner electrodes. The capacitor is depicted at a 0° orientation, relative to the circuit board bending (dashed line).

Manuscript received December 20, 2016; revised April 21, 2017; accepted May 12, 2017. Date of publication June 9, 2017; date of current version November 16, 2017. *(Corresponding author: Saku Levikari.)*

S. Levikari, T. J. Kärkkäinen and P. Silventoinen are with the LUT School of Energy Systems, Lappeenranta University of Technology, 53850 Lappeenranta, Finland (e-mail: saku.levikari@student.lut.fi; tommi.karkkainen@lut.fi; pertti.silventoinen@lut.fi).

C. Andersson is with ABB Corporate Research Center, 5405 Baden-Dättwil, Switzerland (e-mail: caroline.andersson@ch.abb.com).

J. Tamminen is with ABB Drives, FI-00381 Helsinki, Finland (e-mail: juha.tamminen@fi.abb.com).

Color versions of one or more of the figures in this paper are available online at http://ieeexplore.ieee.org.

Digital Object Identifier 10.1109/TIE.2017.2714123

0278-0046 © 2017 IEEE. Translations and content mining are permitted for academic research only. Personal use is also permitted, but republication/redistribution requires IEEE permission. See http://www.ieee.org/publications_standards/publications/rights/index.html for more information.

nant ultrasound spectroscopy. The interest in acoustic methods is explained by the fact that they are quick to apply and nondestructive for the capacitors. Therefore, they could potentially be further refined into a production line screening method. Other known methods, such as capacitance or leakage current monitoring, are based on detecting anomalies in the electrical operation of the capacitor; the acoustic method does not need leakage current, as mechanical defects can be detected even if the electrical operation of the capacitor is normal. The earlier work on acoustic phenomena of other electronic components, especially for the condition monitoring of power semiconductor modules [21]–[24], has also yielded important results on acoustic inspection and analysis methods.

Krieger *et al.* did their work on MLCCs that were soldered on a PCB [12]. The vibrations were induced in the capacitors by an electrical frequency sweep signal applied to them. The vibration measurements were not carried out directly on the capacitors. Johnson *et al.* [19], [20] conducted their measurements directly on the capacitors, but the capacitors were not assembled on a circuit board. It can be argued that the experimental setup of Krieger *et al.* has more resemblance to a production testing environment, but the measurements performed by Johnson *et al.* provide a better acoustic representation of the capacitor itself. In this study, vibrations are measured directly from capacitors that are soldered onto a PCB, and the vibrations are induced by an electrical signal applied to the capacitor.

In the present study, MLCCs were driven with pulse wave frequency sweeps to excite acoustic emissions, which were measured directly from the component using a piezoelectric point contact sensor. First, reference measurements were made for intact capacitors, after which the PCBs were bent once to induce flex cracks to the capacitors. The same capacitors were then remeasured, and the acoustic signatures were compared with the prebending data. The capacitors were also X-ray imaged after bending to verify the presence or absence of cracks. A portion of the capacitors was also cross-sectioned and inspected with an optical microscope in order to detect small cracks and delaminations.

The results show that bending the PCB and the subsequent damage to the MLCC alters the acoustic response of the capacitors. The changes in the acoustic behavior are more significant in capacitors that are damaged than in those that remain intact. This paper also presents conclusions on how the acoustic research of MLCCs could be done in the future. New experiments and research questions are proposed.

II. Acoustic Emission Generation in MLCCs

Acoustic emission generation in MLCCs is a well-known phenomenon [1]. It is caused by piezoelectric behavior of barium titanate ($BaTiO_3$), which is a typical dielectric material in type II MLCCs [25], [26]. When subjected to ac voltage, an MLCC starts to vibrate, and the vibration amplitude is greater near the resonance frequencies of the MLCC body. Ko *et al.* performed a modal analysis for a typical MLCC, for which the first four modes were found at 1.46, 1.47, 1.48, and 2.27 MHz corresponding to out-of-plane, in-plane, torsional, and compressional vibration. As the MLCC is small and lacks audio range resonances, the capacitor itself cannot produce significant audible noise, which is caused as the circuit board starts to vibrate [1]. Therefore, acoustic emissions should be measured directly from the component to bypass any effect of PCB resonances and sound damping caused by air. PCB-bending-related cracks, i.e., flex cracks, in the ceramic material of an MLCC decrease the stiffness of the component body. Thus, an amplitude increase in the resonance peaks can be considered a sign of damage or defect in the capacitor [17], [18].

TABLE I
Test Board Specifications

Material	FR-4
Dimensions	39.0 cm by 30.4 cm
Thickness	1.55 mm
Copper layers	2
Coatings	None
Solder	SAC: 96.5Sn-3.0Ag-0.5Cu

III. Experiment

The goal of the measurements was to observe mechanical vibrations and resonances of MLCCs directly from the components themselves with a point contact sensor. The capacitors were assembled on test boards, which were bent once to a selected strain level to induce flex cracks in the capacitors. The MLCCs were measured acoustically before and after bending, and the measurement data were processed in order to find bending-related differences.

A. MLCCs and Test Board Setup

MLCCs from three different manufacturers were used for the experiments. A total of 240 capacitors were tested, including both normal (or standard) and flexible (or soft) termination MLCCs, with case sizes 1206, 1210, 1812, and 2220. The capacitors were assembled on two test boards with specifications shown in Table I. The capacitors were assembled in 12 columns per board. Each column comprised ten MLCCs with equivalent specifications, as shown in Table II. The capacitor orientation is defined in Fig. 1.

B. Measurement Equipment

Acoustic emissions were measured from the top surface of the MLCCs using a KRN Services KRNBB-PC piezoelectric point contact sensor, which has a frequency range of up to 2.5 MHz. The sensor was attached to a 3-D-printed fixture shown in Fig. 2, and the contact point was covered with Kapton tape to prevent shorting out of the capacitor. The sensor was connected to a Keysight InfiniiVision MSO-X 4104A oscilloscope through a KRN AMP-1BB-J preamplifier. The measurement setup was assembled in an anechoic room to minimize any external acoustic interference.

C. Experimental Procedure

The MLCCs on the test boards were acoustically characterized by driving the capacitors with pulse wave frequency sweeps

TABLE II
DETAILS OF MLCCS ON TEST BOARDS

	Column	Case (Normal/Flex)	C (μF)	Orientation
Test board 1	a	1206 N	4.7	0°
	b	1206 F	4.7	0°
	c	1206 N	4.7	45°
	d	1206 F	4.7	45°
	e	1206 N	4.7	90°
	f	1206 F	4.7	90°
	g	1210 N	10	0°
	h	1210 F	10	0°
	i	1210 N	10	45°
	j	1210 F	10	45°
	k	1210 N	10	90°
	l	1210 F	10	90°
Test board 2	a	1812 N	22	0°
	b	1210 F	10	0°
	c	1812 N	22	45°
	d	1210 F	10	45°
	e	1812 N	22	90°
	f	1210 F	10	90°
	g	2220 N	22	0°
	h	2220 F	22	0°
	i	2220 N	22	45°
	j	2220 F	22	45°
	k	2220 N	22	90°
	l	2220 F	22	90°

All capacitors rated at 25 V.

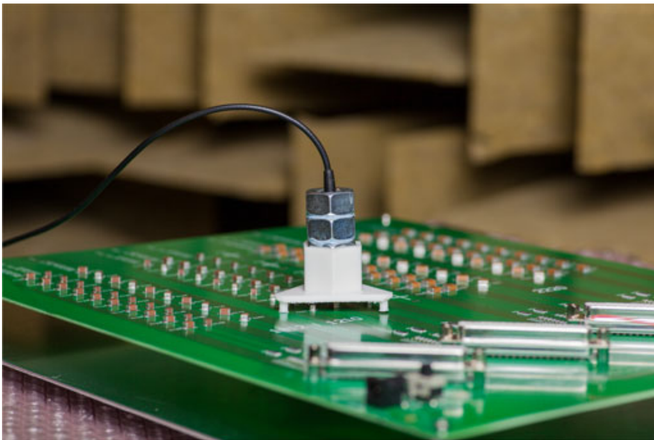

Fig. 2. KRN point contact sensor inside a 3-D-printed fixture placed on top of an MLCC, with four hex nuts for additional weight.

from 100 Hz to 2 MHz while measuring acoustic emissions. A pulse wave with an amplitude of ± 10 $\mathrm{V_{peak}}$ and a duty cycle of 80% was used, as it yielded a higher acoustic response than a sine or square wave. A high duty cycle causes the dc offset to the waveform, polarizing the ceramic dielectric and facilitating acoustic emission generation in MLCCs [12]. The duration of the sweep was set to 100 ms for a sufficiently high oscilloscope sampling rate.

The test boards were bent using a Zwick/Roell Z010 four-point bending setup, described in detail in [16]. The PCBs were subjected to an 18-mm bending displacement, corresponding to an average strain level of 6000 μStr, with values ranging from 5800 to 8000 μStr. The bending strain was measured at four positions at the centerline of the board, and it was higher at the edges of the board. After a single bending, the test boards were removed from the bending setup, and all the capacitors were examined by X-ray imaging to reveal cracks. Both end terminations of each MLCC were imaged at a 70° tilt angle using a Phoenix Nanomex X-ray machine. The X-ray imaging procedure is described in [16]. The same capacitors were then recharacterized acoustically without *a priori* information about the X-ray inspection results. Later, all the 120 capacitors on Test board 2 were cross-sectioned and polished, and then imaged using an optical microscope. For some of the MLCCs, the cross-sectioning was done to multiple depths. Because cross-sectioning is very laborious and therefore expensive, only one board was chosen for the procedure.

D. Numerical Comparison of Acoustic Signal Envelopes

An algorithm for numerical comparison of MLCC acoustic responses was developed. The algorithm was based on obtaining an envelope curve of the measured acoustic signal. This method provides a smooth curve, which neglects phase differences between measurements while maintaining the amplitude information.

First, frequencies up to 40 kHz were cut off from the measured signal, because a high-amplitude burst occurred in this frequency range. The burst was caused by vibration of the PCB and showed large variation in amplitude between measurements. The envelope $e(t)$ was then calculated for each measured signal $u(t)$ as

$$e(t) = \mathrm{Downsample}_{N_{\mathrm{DS}}}\left\{ \mathrm{lpf}\left[\sqrt{\left(u(t)\right)^2 + \mathrm{Re}\left\{\mathcal{H}\left(u(t)\right)\right\}^2} \right] \right\} \tag{1}$$

where $\mathcal{H}\big(u(t)\big)$ is the Hilbert transform of the signal, lpf is a second-order Butterworth-type low-pass filter with a cutoff frequency of 8 kHz, and N_{DS} is a downsampling factor of 80. Here, e and u are treated as vectors containing the discrete data points of the signals.

It was assumed that all the intact capacitors with equivalent specifications have a similar acoustic response, because the resonant frequencies of a capacitor depend on its physical dimensions and mechanical properties. Krieger *et al.* also observed that the acoustic spectra of defect-free capacitors are similar to each other [12], which supports our assumption. Therefore, a reference envelope for each capacitor column (see Table II) was formed by calculating the mean and standard deviation of the prebending envelopes e in the column. Such a statistical approach was chosen because it minimizes the effect of outliers and provides information on the variation within the reference data.

It was observed that the amplitude of the envelope is dependent on the contact and downward force of the sensor. This dependence was modeled as

$$e = e_{\mathrm{ref}}\theta + v \tag{2}$$

where $\theta \in \mathbb{R}_+$ depends on the mechanical contact between the sensor and the MLCC, and v is a zero-mean error vector. To reduce the variation caused by the mechanical contact, the mean

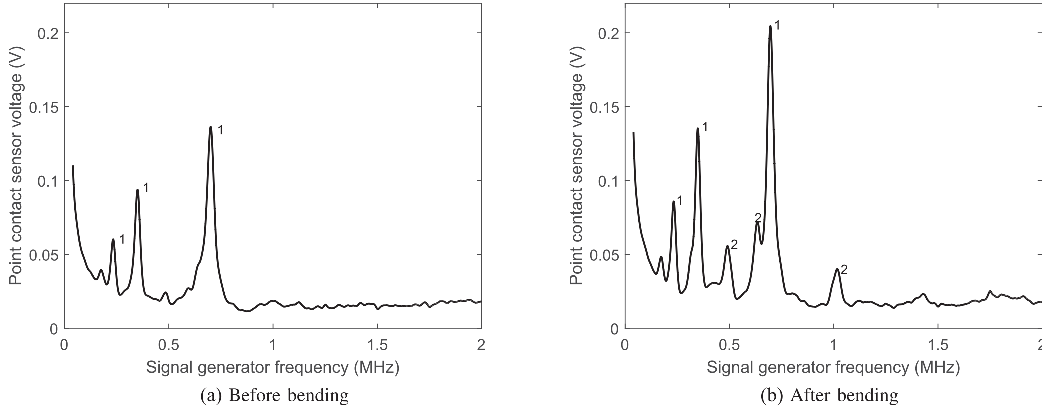

Fig. 3. Typical acoustic response of a 1812-size MLCC before (a) and after (b) a single PCB bending. The amplitude of the highest resonant peaks increases from 136 to 204 mV (+50%), and the peak shifts from 700.9 kHz to 696.4 kHz (− 6.5%). The difference between (a) and (b) indicates that the mechanical properties of the capacitor body have been affected by test board bending.

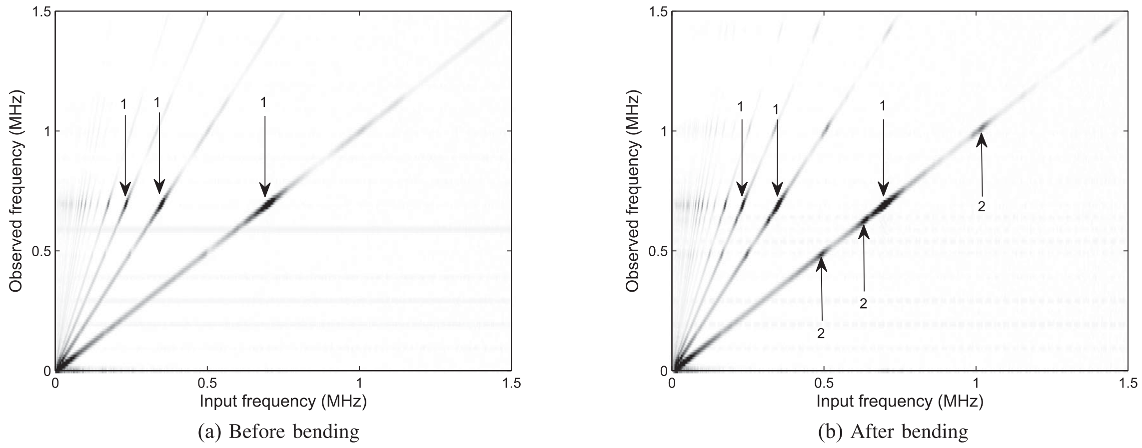

Fig. 4. Spectrograms of the acoustic responses in Fig. 3 before and after a single PCB bending. It is seen that the peaks indicated by “1” in Fig. 3 are different harmonics of one resonant mode, whereas peaks indicated by “2” are all individual resonant modes.

reference envelope was fitted into each envelope of the examined MLCCs using the method of generalized least squares (GLS):

$$\hat{\theta}_{\text{GLS}} = \left(e_{\text{ref}}^{\text{T}} W e_{\text{ref}}\right)^{-1} e_{\text{ref}}^{\text{T}} W e \tag{3}$$

where the inverse variances σ_i^{-2} of the reference envelope were used as weights:

$$W = \text{diag}\left(\frac{1}{\sigma_1^2}, \ldots, \frac{1}{\sigma_N^2}\right). \tag{4}$$

The difference value between the envelope e of the examined MLCC and the least-squares (LS)-fitted reference envelope $\hat{e}_{\text{ref}} = e_{\text{ref}}\hat{\theta}$ was calculated as

$$L_{\text{GLS}} = \frac{\sum_{i=1}^{N} \frac{1}{\sigma_{\text{ref,i}}^2} \left(e_i - \hat{e}_{\text{ref},i}\right)^2}{N \mu_{L_{\text{GLS}},\text{ref}}}. \tag{5}$$

The equation above has been scaled with the number of data points N and the mean of L_{GLS} values of the intact capacitors in the column, $\mu_{L_{\text{GLS}},\text{ref}}$.

Thus, the value of $L_{\text{GLS}} = 1$ corresponds to the reference envelope itself, and the L_{GLS} values for intact capacitors represent the difference between an individual reference MLCC and the mean of reference capacitors. Bending-related changes, such as new resonant peaks, cause an increase in the L_{GLS} values.

IV. Results

A. Effects of PCB Bending on Acoustic Responses

A typical acoustic response of an intact capacitor is shown in Fig. 3(a), which depicts several peaks caused by the mechanical resonance of the capacitor body. Compared with the response of the same MLCC after suffering flex cracks from bending [see Fig. 3(b)], two main features can be associated with the induced cracks: an amplitude increase of resonant peaks (indicated by “1”) and emergence of new resonant peaks (indicated by “2”). Such features were typically not observed in uncracked capacitors. Alongside the amplitude increase, slight shift in acoustic resonant frequencies was also observed in many capacitors (see Fig. 3). These findings are very similar to those made by Johnson *et al.* [19], [20].

The harmonic components of the input signal cause resonant peaks of the capacitor to appear several times during the sweep. A prebending spectrogram in Fig. 4(a) shows that peaks indicated by “1” in Fig. 3(a) are caused by a single vibration mode

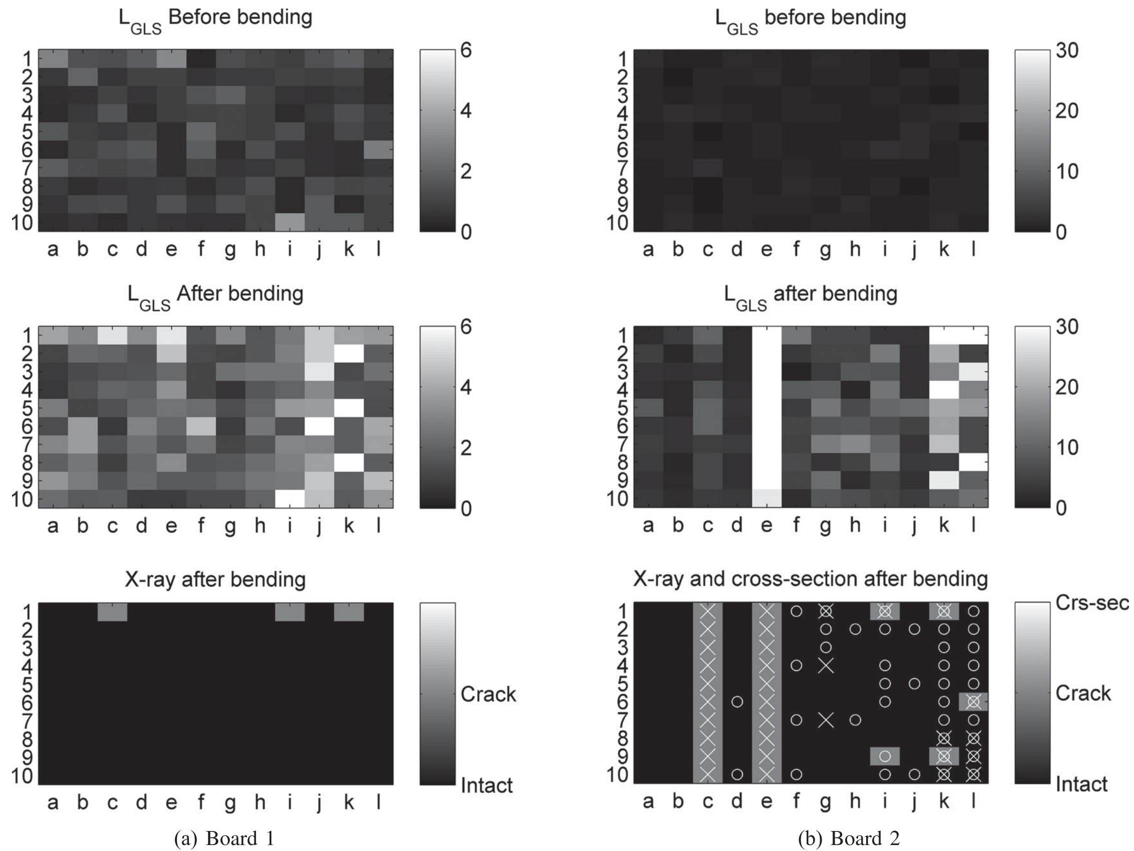

Fig. 5. From top to bottom: Calculated $L_{\rm GLS}$ values before and after 6000 μStr bending, and X-ray-observed cracks (in gray) on Boards 1 and 2. The $L_{\rm GLS}$ values are proportional to the difference between the acoustic response of an individual capacitor and the average acoustic response of that capacitor type. The color scales are different for Boards 1 and 2, as Board 2 yielded a wider range of $L_{\rm GLS}$ values. Additionally, the bottom-right figure shows the results of a cross-sectional analysis performed on Board 2: cracks are indicated by "X" and delaminations by "O." The capacitors on Board 1 were not cross-sectioned.

at 0.7 MHz. The peaks indicated by "2" in Fig. 3(b), instead, are all individual vibration modes, as seen from the corresponding spectrogram [see Fig. 4(b)].

In the damaged capacitors, new resonant peaks typically emerged at specific frequencies, similarly among capacitors of the same case size. These vibration modes become observable because cracks in the ceramic body reduce the stiffness of the capacitor [17], [18].

B. Population-Level Observations

In order to evaluate if the changes in the signals are statistically significant, acoustic data from 240 capacitors were analyzed and compared before and after a single bending. Changes in the acoustic response of an individual capacitor were characterized by comparing the postbending acoustic response with the prebending reference response using the $L_{\rm GLS}$ calculation in (5). The general increase in $L_{\rm GLS}$ values across both test boards (see Fig. 5) indicates that bending the PCB changes the capacitor acoustic responses at the population level. Because this is an early-phase study, the capacitor population comprises various MLCCs with distinct acoustic responses. Therefore, no fixed $L_{\rm GLS}$ limits were set to categorize the capacitors either as damaged or intact.

To see how well the $L_{\rm GLS}$ values correlate with damage, the capacitors on both boards were inspected for cracks by X-ray analysis. Significant acoustic changes were observed in the majority of cracked MLCCs. However, changes were also observed in a number of 2220-sized capacitors that showed no damage in the X-ray. Therefore, all the MLCCs on Board 2 were cross-sectioned, revealing several cracks that were not identified by the X-ray inspection. A number of delaminated capacitors were also observed, as delamination cannot be detected by the X-ray method. The experimental cumulative distribution in Fig. 6 shows that the $L_{\rm GLS}$ values for intact, damaged, and cracked groups differ in a statistically significant way. Thus, it can be concluded that the damage in the capacitors changes the acoustic behavior. The cracked capacitors appear to form two distinct groups, although this can probably be attributed to the relatively low number of samples.

Remarkably, the postbending $L_{\rm GLS}$ distribution for intact capacitors differs from the prebending. This is partly due to the fact that the reference envelope for a prebending measurement contains data from the measured capacitor itself. However, bending may actually change the acoustic behavior of a capacitor without actual damage. Another explanation is that some of the damages in the capacitors were left unidentified in both X-ray analysis and cross-sectioning. It is also possible that the bending of the

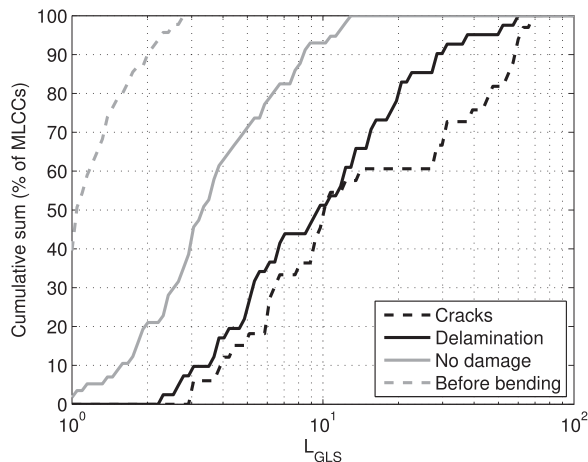

Fig. 6. Experimental cumulative distribution of $L_{\rm GLS}$ values for test board 2 before and after bending. Postbending distribution comprises capacitors that were delaminated and/or cracked, or remained intact. After bending, over 90% of the intact capacitors yielded $L_{\rm GLS}$ values below 10, whereas only 50% of damaged capacitors showed values below 10.

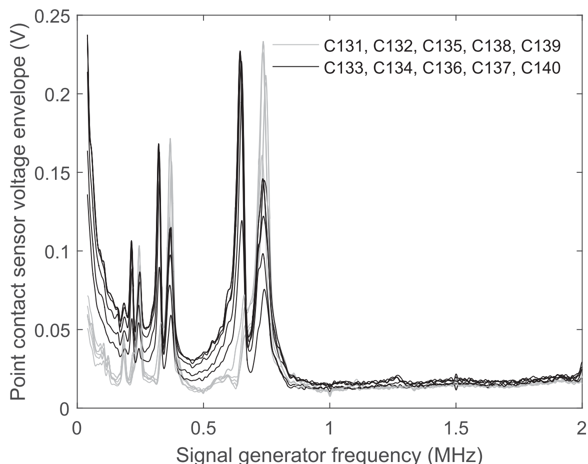

Fig. 7. Differing prebending acoustic responses of MLCCs from Board 2, column b (1210 case, flexible termination). Similar behavior was also observed in some 1210-sized MLCCs with normal terminations.

PCB causes metal fatigue in the end terminations, solder, or the circuit board, which may alter the acoustic characteristics. Still, capacitors with actual observed damage show clearly higher $L_{\rm GLS}$ values than those where none are observed.

The 1206-sized capacitors showed little change in the $L_{\rm GLS}$ values after bending (see Fig. 5(a), columns a–f). In the X-ray analysis, cracks were found only in capacitor $c1$, which also showed significantly increased $L_{\rm GLS}$ values, meaning that the damage was observed acoustically.

The 1210-sized capacitors showed very nonuniform acoustic responses both before and after bending. The number and size of resonance peaks varied between the MLCCs, with typically either one or two large peaks found near 750 kHz (see Fig. 7). This behavior makes the numerical comparison of envelopes fairly inaccurate, as the reference envelope $\hat{e}_{\rm ref}$ in (5) comprises dissimilar acoustic responses. As such, the few damaged capacitors in Fig. 5(a) (columns f–l) and Fig. 5(b) (columns d, b, and f) cannot be identified based on their $L_{\rm GLS}$ values. This nonuniform acoustic behavior should be taken into account in future studies.

The highest proportion of cracks was found in the 1812-sized capacitors, which also showed the best correspondence between $L_{\rm GLS}$ values and cracks (see Fig. 5(b), columns a, c, and e). The orientation of these capacitors correlated with the size of the cracks, and this correlation was also seen from the acoustic changes. No cracks were found in the 0°-oriented capacitors, which also yielded the lowest $L_{\rm GLS}$ values (column a). Small cracks, covering the width of the ceramic body only partially [see Fig. 8(a)], were found in column c (45°). Larger, full-width cracks [see Fig. 8(b)] were present in the 90°-oriented capacitors in column e; in some cases, the cracks also extended into the solder joint. However, there were not enough solder cracks to discuss them as a separate statistical population. The corresponding $L_{\rm GLS}$ values are higher for the capacitors with larger cracks, suggesting that it might be possible to evaluate the crack size acoustically.

Only five of the 2220-sized MLCCs showed cracks in the X-ray, which contradicted the elevated $L_{\rm GLS}$ values (see Fig. 5(b), columns g–l). Cross-sectioning revealed a number of delaminated capacitors, plus additional cracks that were left undetected in the X-ray. Because cross-sectioning only provides information about a capacitor at one depth, it could not be used to quantify the damage. Furthermore, the inspection was done by eye, and thus, misidentifications are possible. However, the delaminations were largest and clearest in the 90°-oriented MLCCs in columns k and l, where also the highest $L_{\rm GLS}$ values were found. This further supports the finding that the degree of acoustic changes could correlate with the size of damage inflicted on a capacitor.

C. Interference and Uncertainty in Acoustic Measurements

Because the capacitors were simultaneously electrically excited and acoustically measured, the measurement data contained electromagnetic interference (EMI). Moreover, any external acoustic disturbances could cause artifacts in the acoustic data, thereby skewing the numerical comparison. The effect of external acoustic noise sources was minimized by performing the measurements in an anechoic room. However, the circuit board itself was observed to vibrate, causing a notable acoustic burst at the beginning of each sweep. The PCB vibrations were observable up to 40 kHz (see Fig. 9), and thus, frequencies below this were cut off from the measured acoustic signals. Above 40 kHz, the noise floor was dictated by the EMI from the measurement setup. The signal-to-noise ratio (SNR) of the acoustic signal was dependent on the capacitor size as the surface displacement of an MLCC is affected by its electrical and mechanical properties (see Table III). The 2220-sized MLCCs yielded the lowest acoustic resonance peaks, reducing the precision of the $L_{\rm GLS}$ comparison.

Furthermore, the general amplitude of the acoustic signals was affected by variations in the mechanical coupling between the sensor and the capacitor. Specifically, the LS fitting in (3) was chosen to counter this variation.

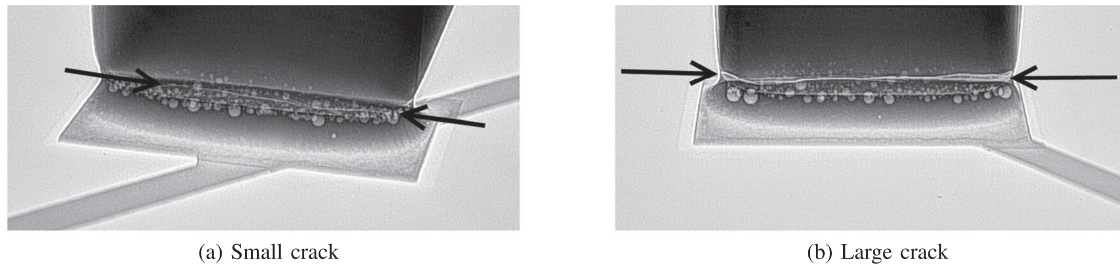

(a) Small crack (b) Large crack

Fig. 8. X-ray images of MLCC end terminations, showing flex cracks (endpoints indicated by arrows). The capacitor in (a) was oriented at a 45° angle relative to the bending direction, resulting in a narrower crack than in (b), oriented at 90°. Capacitors with wider cracks also showed higher acoustic changes. The damage seen in (a) is typical for capacitors in column c in Fig. 5(b), whereas cracks like in (b) were found in column e capacitors in Fig. 5(b).

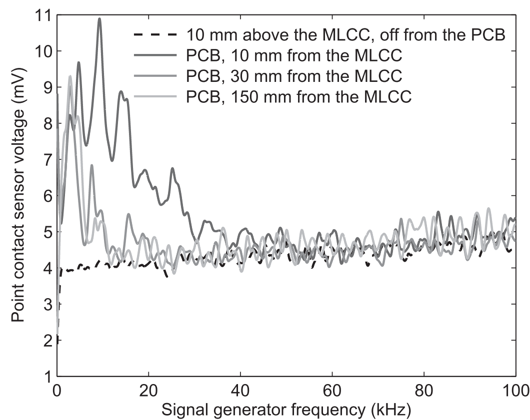

Fig. 9. Acoustic emissions measured from PCB surface and above an MLCC. The results show that vibration of the test board has very little effect on the measured acoustic emissions above 40 kHz.

TABLE III
MEAN AND STANDARD DEVIATION OF ACOUSTIC EMISSION PEAK VOLTAGES FOR INTACT MLCCS

Case size	Mean (e_{peak})(V)	Std (e_{peak})(V)	Std (%)
1206	0.0874	0.0247	28
1210	0.1588	0.0447	28
1812	0.1230	0.0237	19
2220	0.0284	0.0052	18

V. DISCUSSION

The results show that MLCC acoustic behavior can be characterized by using a piezoelectric sensor, and this behavior is altered by circuit board bending. In individual capacitors, the changes are seen as an increased amplitude of mechanical resonance peaks and introduction of new peaks. Furthermore, when the typical acoustic behavior of a capacitor is known, a single capacitor can be numerically compared with a reference waveform of that particular type of capacitor.

Both cracks and delaminations produced changes in the acoustic signatures of the capacitors. The magnitude of these changes was observed to somewhat correlate with the size of damage found in a capacitor, although quantifying the damage was not feasible. The population-level increase in the L_{GLS} values of damaged capacitors shows that cracks and delaminations can be identified acoustically. Machine learning and more advanced feature extraction tools could be implemented for more precise damage detection, although a more exhaustive sample of MLCCs is also needed. It can be assumed that cracks and delaminations affect the mechanical properties in different ways. Thus, it might be possible to acoustically differentiate between a cracked and a delaminated capacitor; this is a subject for further research.

Because the EMI noise from the excitation signal occurs at the same frequency with the acoustic emissions, simple low-pass filtering is not feasible. A more advanced denoising method (e.g., wavelet-based) could be applied to improve the SNR. Moreover, the measurement setup should be improved for better EMI shielding and more consistent sensor–capacitor contact. Because the frequency range of the sensor used in this study is limited to 2.5 MHz, a sensor with a higher frequency range should be used if capacitors of a smaller case size (e.g., 0603) were to be measured.

VI. CONCLUSION

Direct measurements of acoustic emissions from MLCCs were demonstrated using a piezoelectric point contact sensor. MLCCs were measured both pristine and after damaging them by bending the test circuit boards once. The acoustic measurements were then compared with X-ray and cross-section images. The results show that mechanical damage, such as flex cracks and delaminations, changes the acoustic behavior of the MLCCs. The acoustic changes in capacitors were characterized with a numerical algorithm, showing that the circuit board bending affects the acoustic response of the MLCCs at the population level in a statistically significant way. Furthermore, it appears that the degree of acoustic changes correlates with the level of physical damage to the capacitor. In the light of these results, an acoustic emission-based defect detection method for MLCCs could be developed. Still, the precision and error sensitivity of the acoustic measurements leave room for improvement. Additionally, the relationship between the acoustic signatures and the quality of damage in capacitors is a subject for further work.

REFERENCES

[1] B.-H. Ko, S.-G. Jeong, Y.-G. Ahn, K.-S. Park, N.-C. Park, and Y.-P. Park, “Analysis of the correlation between acoustic noise and vibration generated by a multi-layer ceramic capacitor,” *Microsyst. Technol.*, vol. 20, pp. 1671–1677, 2014.

[2] C.-W. Huang, B.-T. Chen, K.-Y. Chen, C.-H. Hsueh, W.-C. Wei, and C.-T. Lee, "Finite element analysis and design of thermal-mechanical stresses in multilayer ceramic capacitors," *Int. J. Appl. Ceramic Technol.*, vol. 12, no. 2, pp. 451–460, Mar. 2015.

[3] T. Adams, "Preventing MLCC failures," *Circuits Assembly*, vol. 20, p. 17, Aug. 2009.

[4] J. Bergenthal and J. D. Prymak, "Capacitance monitoring while flex testing," in *Proc. 44th Electron. Compon. Technol. Conf.*, May 1994, pp. 854–860. [Online]. Available: http://dx.doi.org/10.1109/ECTC.1994.367528

[5] J. A. Ahmar and S. Wiese, "A finite element modelling and fracture mechanical approach of multilayer ceramic capacitors," in *Proc. 16th Int. Conf. Thermal, Mech. Multi-Phys. Simul. Exp. Microelectron. Microsyst.*, 2015, pp. 1–5.

[6] T. Adams, "High acoustic frequency imaging," *Ceramic Ind.*, vol. 164, no. 2, pp. 14–16, 2014.

[7] S. Kahn and R. Checkaneck, "Acoustic emission testing of multilayer ceramic capacitors," *IEEE Trans. Compon., Hybrids, Manuf. Technol.*, vol. CHMT-6, no. 4, pp. 517–526, Dec. 1983. [Online]. Available: http://dx.doi.org/10.1109/TCHMT.1983.1136222

[8] J. M. J. den Toonder, C. W. Rademaker, and C. Hu, "Residual stresses in multilayer ceramic capacitors: Measurement and computation," *J. Electron. Packag.*, vol. 125, no. 4, pp. 506–511, 2003.

[9] G. Vogel, "Avoiding flex cracks in ceramic capacitors: Analytical tool for a reliable failure analysis and guideline for positioning cercaps on PCBs," *Microelectron. Rel.*, vol. 55, pp. 2159–2164, Jun. 2015.

[10] L. Bechou, S. Mejdi, Y. Ousten, and Y. Danto, "Non-destructive detection and localization of defects in multilayer ceramic chip capacitors using electromechanical resonances," *Quality Rel. Eng. Int.*, vol. 12, pp. 43–53, 1996.

[11] W. L. Johnson, S. A. Kim, G. S. White, J. Herzberger, K. L. Peterson, and P. R. Heyliger, "Time-domain analysis of resonant acoustic nonlinearity arising from cracks in multilayer ceramic capacitors," *Proc. AIP Conf. Proc.*, vol. 1706, 2016, Art. no. 060005. [Online]. Available: http://dx.doi.org/http://dx.doi.org/10.1063/1.4940511

[12] V. Krieger, W. Wondrak, A. Dehbi, W. Bartel, Y. Ousten, and B. Levrier, "Defect detection in multilayer ceramic capacitors," *Microelectron. Rel.*, vol. 46, no. 9, pp. 1926–1931, 2006. [Online]. Available: http://dx.doi.org/http://dx.doi.org/10.1016/j.microrel.2006.07.082

[13] Y. C. Chan, F. Yeung, G. Jin, N. Bao, and P. S. Chung, "Nondestructive detection of defects in miniaturized multilayer ceramic capacitors using digital speckle correlation techniques," *IEEE Trans. Compon., Packag., Manuf. Technol. A*, vol. 18, no. 3, pp. 677–684, Sep. 1995.

[14] D. L. Commare, "Nondestructive evaluation of MLCCS," *Ceramic Ind.*, vol. 140, no. 6, pp. 38–41, 1993.

[15] G. F. Kieran, "A comparison of screening techniques for ceramic capacitors," in *Capacitor Technologies, Applications and Reliability*. Huntsville, AL, USA: Marshall Space Flight Center, Feb. 1981, pp. 111–117.

[16] C. Andersson, J. Ingman, E. Varescon, and M. Kiviniemi, "Detection of cracks in multilayer ceramic capacitors by x-ray imaging," *Microelectron. Rel.*, vol. 64, pp. 352–356, 2016. [Online]. Available: http://dx.doi.org/http://doi.org/10.1016/j.microrel.2016.07.110

[17] D. S. Erdahl and I. C. Ume, "Online-offline laser ultrasonic quality inspection tool for multilayer ceramic capacitors—part I," *IEEE Trans. Adv. Packag.*, vol. 27, no. 4, pp. 647–653, Nov. 2004.

[18] D. S. Erdahl and I. C. Ume, "Online-offline laser ultrasonic quality inspection tool for multilayer ceramic capacitors-part ii," *IEEE Trans. Adv. Packag.*, vol. 28, no. 2, pp. 264–272, May 2005.

[19] W. L. Johnson, S. A. Kim, G. S. White, and J. Herzberger, "Nonlinear resonant acoustic detection of cracks in multilayer ceramic capacitors," in *Proc. IEEE Int. Ultrason. Symp.*, Sep. 2014, pp. 244–247, [Online]. Available: http://dx.doi.org/10.1109/ULTSYM.2014.0062

[20] W. I. Johnson, J. L. Herzberger, S. A. Kim, K. L. Peterson, P. R. Heyliger, and G. S. White, "Resonant acoustic frequency shifts associated with cracks in multilayer ceramic capacitors," *IEEE Trans. Device Mater. Rel.*, vol. 17, no. 2, pp. 316–323, Jun. 2017. http://dx.doi.org/10.1109/TDMR.2017.2682818

[21] T. J. Kärkkäinen *et al.*, "Acoustic emission in power semiconductor modules—First observations," *IEEE Trans. Power Electron.*, vol. 29, no. 11, pp. 6081–6086, Nov. 2014. [Online]. Available: http://dx.doi.org/10.1109/TPEL.2013.2295460

[22] T. J. Kärkkäinen, J. P. Talvitie, O. Ikonen, M. Kuisma, P. Silventoinen, and E. Mengotti, "Sounds from semiconductors—Acoustic emission experiment with a power module," in *Proc. 16th Eur. Conf. Power Electron. Appl.*, Aug. 2014, pp. 1–6. [Online]. Available: http://dx.doi.org/10.1109/EPE.2014.6910840

[23] T. J. Kärkkäinen, J. P. Talvitie, M. Kuisma, P. Silventoinen, and E. Mengotti, "Acoustic emission caused by the failure of a power transistor," in *Proc. IEEE Appl. Power Electron. Conf. Expo.*, Mar. 2015, pp. 2481–2484. [Online]. Available: http://dx.doi.org/10.1109/APEC.2015.7104697

[24] S. Müller, C. Drechsler, U. Heinkel, and C. Herold, "Acoustic emission for state-of-health determination in power modules," in *Proc. 13th Int. Multi-Conf. Syst., Signals Devices*, Mar. 2016, pp. 468–471. [Online]. Available: http://dx.doi.org/10.1109/SSD.2016.7473704

[25] J. D. Prymak, "Piezoelectric effects ceramic chip capacitors (singing capacitors)," *Arrow Asian Times*, KEMET Electronics Corp., 2006.

[26] J. Chen and Z. Feng, "X7R dielectric multilayer ceramic capacitors show good micro-actuating properties with little hysteresis," *Electron. Lett.*, vol. 50, no. 7, pp. 538–540, 2014. [Online]. Available: http://dx.doi.org/10.1049/el.2013.3815

Saku Levikari was born in Finland in 1991. He is currently working toward the master's degree in acoustic evaluation of multilayer ceramic capacitors with the Laboratory of Applied Electronics, Lappeenranta University of Technology, Lappeenranta, Finland.

Tommi J. Kärkkäinen (M'12) was born in Finland in 1987. He received the B.Sc., M.Sc., and D.Sc. degrees from Lappeenranta University of Technology (LUT), Lappeenranta, Finland, in 2010, 2011, and 2015, respectively.

He is currently a Postdoctoral Researcher with LUT School of Energy Systems. His main research interests include the utilization of acoustic phenomena to the condition monitoring and health testing of electronics components, and related metrology and signal processing.

Caroline Andersson (M'10) was born in Sweden in 1983. She received the M.Sc. degree in engineering from Lund University, Lund, Sweden, in 2007, and the Ph.D. degree in passivation of Ge for high mobility CMOS transistors from the Swiss Federal Institute of Technology, Zurich, Switzerland, in 2012.

She is currently working as a Senior Scientist with ABB Corporate Research Center, Baden-Dättwil, Switzerland, on the topic of reliability of power electronics. Her research interests include accelerated life testing, physics of failure, and reliability of components and systems.

Juha Tamminen was born in Finland in 1980. He received the B.Eng. degree in electronics from Espoo-Vantaa University of Applied Sciences, Espoo, Finland, in 2006.

He is currently working as a Design Manager with ABB Drives, Helsinki, Finland, in the field of production testing. His work concentrates on improving production testing concepts in pursue of better quality and productivity.

Pertti Silventoinen (M'09) was born in Simpele, Finland, in 1965. He received the D.Sc. degree from Lappeenranta University of Technology (LUT), Lappeenranta, Finland, in 2001.

He became a Professor of applied electronics with LUT in 2004. His current research interests include power electronics systems in various applications.